Half-Megasecond *Chandra* Spectral Imaging of the Hot Circumgalactic Nebula around Quasar Markarian 231

Stacy H. Teng[1,2], Sylvain Veilleux[3], David S.N. Rupke[4], Roberto Maiolino[5], & Eckhard Sturm[6]

1. NASA Goddard Space Flight Center; 2. NASA Postdoctoral Program Fellow; 3. University of Maryland; 4. Rhodes College; 5. University of Cambridge; 6. MPE

Summary:

A half megaseconds of ACIS-S observation of the nearest known quasar, Mrk 231 (z=0.042), are used to carry out the first ever spatially resolved spectral analysis of a hot X-ray emitting circumgalactic nebula around a quasar. The ~50 x 65 kpc X-ray nebula shares no resemblance with the tidal debris seen at optical wavelengths (Fig. 1). One notable exception is the small tidal arc ~3.5 kpc south of the nucleus where excess soft X-ray continuum emission and Si XIII 1.8 keV line emission are detected, consistent with star formation and its associated alpha-element enhancement, respectively. An X-ray shadow is also detected at the location of the 15-kpc northern tidal tail, implying a foreground hydrogen column density of at least 2.5 x 10^{21} cm^{-2}. The hard X-ray continuum emission within ~6 kpc of the center is consistent with being due entirely to the bright central AGN and the wings of the *Chandra* point spread function. The soft X-ray spectrum of the outer (> 6 kpc) portion of the nebula is best described as the sum of two thermal components of temperatures ~2 and ~7 million K with spatially uniform super-solar alpha-element abundances, relative to iron (Fig. 2). This result implies enhanced star formation activity over ~10^8 years accompanied with redistribution of the metals on large scale. The low-temperature thermal component is not present within 6 kpc of the nucleus, suggesting extra heating in this region from the circumnuclear starburst, the central quasar, or the wide-angle quasar-driven outflow identified from optical IFU spectroscopy on a scale of > 3 kpc. Significant azimuthal variations in the soft X-ray intensity are detected in the inner region where the outflow is present (Fig. 3). The soft X-ray emission is weaker in the western quadrant, coincident with a deficit of H-alpha emission and some of the largest columns of neutral gas outflowing from the nucleus. Shocks created by the interaction of the wind with the ambient ISM may heat the gas to high temperatures at this location. The tentative detection at the ~2-sigma level of He-like Fe XXV 6.7 keV line emission from 70 million K gas extending ~3 kpc north-west of the nucleus provides some support to this scenario, although a contribution from high-mass X-ray binaries cannot be ruled out (Fig. 4).

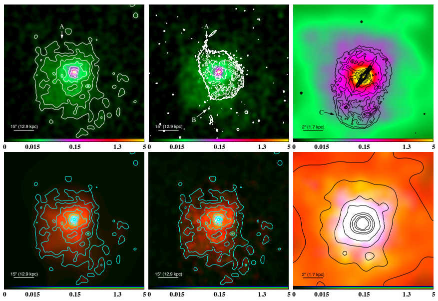

Figure 1: (Top) Adaptively smoothed full X-ray band (0.5 - 8 keV) on a logarithmic scale. North is up and East is to the left. The overlaid contours are (left) the full 0.5-8 keV contours at 2, 3, 5, 10, 25, 50, 100, 500, 1000, and 5000 sigma, (middle) the contours of the optical *HST* image from Rupke & Veilleux (2011), and (right) the contours of the *HST* optical image zoomed in to show the tidal star-forming arc ~3.5 kpc south of the nucleus. The cross-like pattern in the center of the optical image in both the middle and right panels is an artifact of the strong central PSF. Labels A, B, and C point to the northern tidal tail, the southern tidal tail, and the southern tidal arc, respectively. (Bottom) False-color X-ray images of adaptively smoothed images overlaid with the full X-ray band contours from the upper left panel. In all three of these bottom panels, red represents the 0.5 - 1 keV emission, green is 1 - 2 keV, and blue is 2 - 8 keV. The bottom left panel is smoothed using `csmooth` to emphasize the large-scale structure. The middle panel is smoothed using the `imageadapt` script designed to better show the small-scale structures. The bottom right panel is a zoomed-in version of the middle panel.

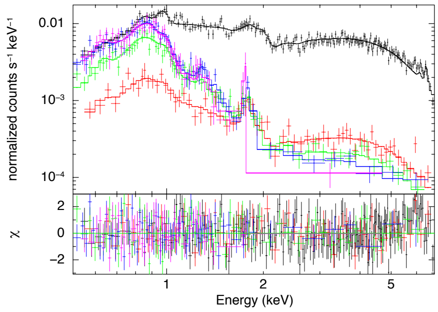

Figure 2: Spectra extracted from annular regions with different radial distances from the nucleus. The nuclear spectrum (r < 1 kpc) is displayed in black, the 1 - 2 kpc (wind region; Fig. 3) spectrum in red, 2 - 6 kpc (starburst arc region; Fig. 3) spectrum in green, 6 - 16 kpc (optical host) spectrum in blue, and 16 - 40 kpc (diffuse X-ray halo) spectrum in magenta. The best-fit model fit simultaneously to all of the spectra is shown. Note the presence of Mg XI 1.352 keV and Si XIII 1.864 keV in the spectra. For the nucleus, the model is the best-fit *NuSTAR+Chandra* MYTorus AGN model (Teng et al. 2014) corrected for the encircled energy of the PSF < 1 kpc. In this model, the direct AGN emission is absorbed and scattered by a patchy absorber with N_H ~1.2 x 10^{23} cm^{-2}. The absorption corrected 2 - 10 keV luminosity for the AGN is ~3 x 10^{42} erg/s. Also included is the HMXB component from the unresolved circumnuclear starburst with an X-ray luminosity consistent with a 140 M_{sun}/yr SFR. The 1 - 2 and 2 - 6 kpc spectra are best-fit with a single MEKAL component with a temperature of 0.67 keV. The 6 - 16 and 16 - 40 kpc spectra are best-fit with an additional 0.27 keV MEKAL component. Furthermore, the 6 - 16 kpc spectrum, coincident with the optical emission, requires an HMXB component that is equivalent to an SFR ~10 M_{sun}/yr. There is no evidence for warm absorbers.

Neutral Outflow Region and the Starburst Arc:

The spatially resolved Na ID outflow detected by Rupke et al. (2005) and mapped by Rupke & Veilleux (2011, 2013) extends to at least ~2.0 - 2.5 kpc, depending on azimuth angle. There is a region ~1.0 - 2.5 kpc due north of the nucleus of Mrk 231 where the Na ID outflow velocities are noticeably higher than along other directions. Rupke & Veilleux (2011) argue that the outflowing neutral gas in this region may be given an extra kick by the radio jet, seen on smaller scale along the same direction (e.g., Carilli et al. 1998; Ulvestad et al. 1999). However, we see no evidence (e.g., higher temperatures) for jet interaction with the ISM in the northern region. We do detect a soft X-ray flux deficit in the western quadrant (Fig. 3).

The Na ID velocity map of Rupke & Veilleux (2011, 2013) also show blue-shifted emission associated with a starburst arc due south of the nucleus. The 2.0 - 4.5 kpc annulus was divided into four quadrants to produce spectra for each region. The soft X-ray emission in the western arc region is significantly weaker than in the other arc regions. In contrast, the hard X-ray emission is very nearly constant, resulting in a higher hardness ratio in the western region. This soft X-ray flux deficit is analogous to the behavior at smaller radii (the western outflow region) and may thus be physically related to the outflow. Significant emission lines are detected near ~1.8 and 1.2 keV in the southern arc region. These features are identified as Si XIII 1.864 keV and Ne X 1.211 keV (or Fe XIX 1.258 keV), respectively. This excess line emission may reflect alpha-element enhancement due to the starburst in the arc region (Fig. 3)

The soft X-ray flux deficit in the western outflow and arc regions is the strongest evidence in our data that the hot X-ray emitting gas "knows" about the massive neutral/molecular outflow. This region coincides with fainter H-alpha emission and some of the largest columns of outflowing neutral gas probed by observations of the Na I optical doublet.

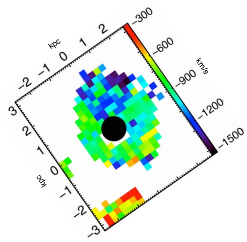

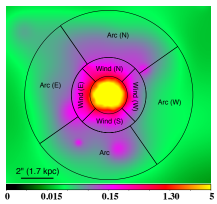

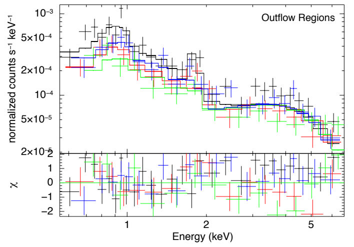

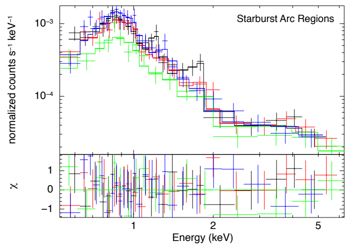

Figure 3: (Above, Left) IFU Na ID velocity map of Mrk 231 from Rupke & Veilleux (2013). In the northern quadrant, the outflowing material appears to receive an additional kick from the jet. (Above, Right) The outflow and tidal arc extraction regions. The northern wind region is coincident with the highest blue-shifted quadrant in the Na ID velocity map and the southern arc region is coincident with the star-forming region to the south of the nucleus. All other quadrants are used as comparison regions. (Right, Top) Spectra extracted from the outflow regions shown with the best-fit model that is simultaneously fit to all spectra. Here, black is east, red is south, green is west, and blue is north. Si XIII 1.864 keV emission is detected in the eastern region. The eastern quadrant also has a slightly softer profile from the other three regions. Rupke & Veilleux (2011, 2013) pointed out the presence of a prominent H II region ~1 kpc due east of the nucleus; this region is likely the source of the excess soft X-ray emission detected in the eastern spectrum. The fit requires super-solar Si abundances that may reflect alpha-element enhancement from star formation within the eastern quadrant. The fits indicate a clear deficit of soft X-rays in the western region which is associated with the faintest H-alpha emission. (Right, Bottom) Spectra extracted from the starburst arc regions shown with the best-fit model that is simultaneously fit to all spectra. The black spectrum is of the arc itself; the red, green, and blue spectra are the eastern, western, and northern comparison spectra, respectively. Significant detections of the Mg XI 1.352 keV and Si XIII 1.864 keV emission lines are seen in the arc spectrum, but nowhere else. These lines indicate the presence of alpha-element enhancement due to the starburst in this region. Note the deficit of soft X-ray emission in the western spectrum, similar to that found in the western wind region.

Narrowband Line Images and Spectra:

We created narrowband line images to investigate the two-dimensional spatial distribution of the line-emitting gas (Fig. 4). We find clear evidence for Si XIII emission outside of the nucleus, extending at least ~5 kpc south of the nucleus. Some of the strongest Si XIII emission coincides with the southern star-forming arc, confirming the results from our spectral analysis (Fig. 3). We do not find convincing evidence for Fe Kalpha emission outside of the nucleus. The slightly more significant extension is seen in the Fe XXV + Fe XXVI line emission map (Fig. 4). This is tantalizing evidence for Fe XXV 6.7 keV line-emitting gas with T ~ 7 x 10^7 K (or, equivalently, shock velocities of ~2200 km/s) extended up to ~3 kpc from the nucleus. However, we cannot rule out contribution from HMXBs.

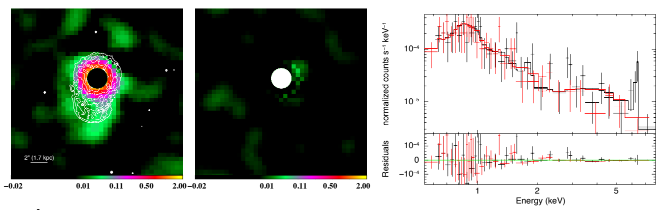

Figure 4: (Left) Continuum-subtracted map of the Si XIII (1.70 - 1.95 keV) compared with the *HST* optical image (contours). The bright continuum emission from the central quasar makes the maps unreliable within the central 3.0 kpc diameter region; this region is masked. Filamentary Si XIII emission is seen out to ~5 kpc. (Center) Continuum-subtracted map of the Fe XXV + Fe XXVI (6.56 - 6.90) keV) emission. Extended Fe XXV + Fe XXVI emission may be present ~3 kpc north-west of the nucleus. (Right) Spectrum (black) extracted from a 2" diameter region centered on the brightest part of the Fe XXV + Fe XXVI extension to the northwest of the nucleus. The spectrum in red is from an equal-size region on the opposite side of the nucleus where there is no obvious emission in the line map. Both spectra are fit with the same continuum model and the Fe emission is very distinct (EW ~ 2.0 keV).

The X-ray Halo:

The soft X-ray spectrum of the nebula beyond 6 kpc is best described as the sum of two thermal components of temperatures ~2 and ~7 million K with spatially uniform super-solar alpha element abundances, relative to iron. A similar result was recently found in the X-ray halo of the pre-merger NGC 6240 (Nardini et al. 2013; Wang et al. 2014). Enhanced star formation activity over an extended period of time (~10^8 years) is needed to produce the vast amount of alpha elements detected in the nebula of Mrk 231. Multiple outflow events, such as the on-going quasar-driven galactic wind, may help carry the alpha elements produced in the circumnuclear region out to the largest scales. Such wind-driven metal transport is directly seen to take place in the nearby starburst M 82, albeit on a considerably smaller scale. The stirring of the gas associated with the merger itself may also redistribute the metals across the nebula and help erase remaining abundance gradients.

A detailed presentation of our analysis and discussion of these results can be found in Veilleux, Teng, Rupke, Maiolino, & Sturm, 2014, ApJ, in press (arXiv:1405.4833).

References:

- Carilli, Wrobel, & Ulvestad, 1998, AJ, 115, 928
- Nardini et al. 2013, ApJ, 765, 141
- Rupke, Veilleux, & Sanders, 2005, ApJ, 632, 751
- Rupke & Veilleux, 2011, ApJ, 729, L27
- Rupke & Veilleux, 2013, ApJ, 768, 75
- Teng et al. 2014, ApJ, 785, 19
- Ulvestad, Wrobel, & Carilli, 1999, ApJ, 516, 127
- Wang et al. 2014, ApJ, 781, 55

Acknowledgements:
Support for this work was provided by NASA through Chandra contract GO2-12129X (S.V.) and the NASA Postdoctoral Program (S.H.T.)